frontiers | Frontiers in Earth Science

TYPE Original Research
PUBLISHED 01 March 2024
DOI 10.3389/feart.2024.1355621

OPEN ACCESS

EDITED BY
Moritz Felix Lehmann,
University of Basel, Switzerland

REVIEWED BY
Mark Alexander Lever,
The University of Texas at Austin, United States
Martin Blumenberg,
Federal Institute For Geosciences and Natural Resources, Germany

*CORRESPONDENCE
Tobias Himmler,
himmler@uni-bremen.de

RECEIVED 14 December 2023
ACCEPTED 15 February 2024
PUBLISHED 01 March 2024

CITATION
Himmler T, Wagner D, Sahy D, Vadakkepuliyambatta S, Chand S, Martma T, Kirsimäe K, Mattingsdal R, Panieri G, Bünz S, Condon DJ, Knies J and Lepland A (2024), Protracted post-glacial hydrocarbon seepage in the Barents Sea revealed by U–Th dating of seep carbonates.
Front. Earth Sci. 12:1355621.
doi: 10.3389/feart.2024.1355621

Protracted post-glacial hydrocarbon seepage in the Barents Sea revealed by U–Th dating of seep carbonates

Tobias Himmler[1,2,3]*, Doris Wagner[4], Diana Sahy[4], Sunil Vadakkepuliyambatta[2,5], Shyam Chand[1,2], Tõnu Martma[6], Kalle Kirsimäe[7], Rune Mattingsdal[8], Giuliana Panieri[2], Stefan Bünz[2], Daniel J. Condon[4], Jochen Knies[1,2] and Aivo Lepland[1,2,6]

[1]Geological Survey of Norway, Trondheim, Norway, [2]Department of Geosciences, Centre for Arctic Gas Hydrate, Environment and Climate, UiT-The Arctic University of Norway, Tromsø, Norway, [3]Fachbereich Geowissenschaften, Universität Bremen, Bremen, Germany, [4]British Geological Survey, Keyworth, United Kingdom, [5]National Centre for Polar and Ocean Research, Ministry of Earth Sciences, Vasco da Gama, India, [6]Department of Geology, Tallinn University of Technology, Tallinn, Estonia, [7]Department of Geology, Tartu University, Tartu, Estonia, [8]Norwegian Petroleum Directorate, Harstad, Norway

The hydrocarbon seepage chronology during deglaciation across the formerly glaciated Barents Sea was established using uranium-thorium (U–Th) dating of seep carbonates. Seep carbonates were sampled with remotely operated vehicles (ROV) from the seafloor at three active hydrocarbon seeps (water depth 156–383 m), located in the north-west (Storfjordrenna), north-central (Storbanken High), and south-west (Loppa High) Barents Sea. Overall, the U–Th dates range from 13.5 to 1.2 thousand years (ka) before present, indicating episodic seep carbonate formation since the late Pleistocene throughout the Holocene. The new U–Th dates indicate protracted post-glacial gas seepage, congruent with previously published seep carbonate ages from the south-west Barents Sea. Gas hydrate dissociation and associated seep carbonate formation occurred at Storfjordrenna between ≈6 and 1.2 ka, and around 13.5 and 6 ka at Storbanken. Early and late Holocene seep carbonate ages from Loppa High support post-glacial seismic activity as potential seepage trigger mechanism.

KEYWORDS

methane, glacial, carbonates, seeps, Barents Sea, U-Th dating

1 Introduction

Hydrocarbon seeps occur on the seafloor where upward migrating hydrocarbon-rich fluids emanate, delivering dissolved and free gas by diffusion and ebullition from the sediment into the seawater (e.g., Suess, 2014). The seeping hydrocarbon fluids can contain methane from various sources, including hydrocarbon reservoirs, free gas accumulations underneath gas hydrate layers, dissociating gas hydrates, or from microbial processes in the shallow subsurface (e.g., Judd et al., 2002; Pohlmann et al., 2009). Before escaping at the seafloor, most of the dissolved methane is typically consumed below the sediment–water interface *via* microbial mediated sulfate-driven anaerobic oxidation of methane (AOM: CH_4

+ SO_4^{2-} → HCO_3^- + HS^- + H_2O) (Boetius et al., 2000; Reeburgh, 2007; and references therein). AOM can also be coupled to the reduction of iron and manganese oxides, making it an effective microbial barrier in marine sediments for upward migrating dissolved methane (Beal et al., 2009; Egger et al., 2018). A consequence of sulfate- and metal-driven AOM is increased pore water carbonate alkalinity through the production of bicarbonate (HCO_3^-), which induces the precipitation of authigenic seep carbonates (e.g., Ritger et al., 1987; Aloisi et al., 2002; Luff et al., 2004; Leefmann et al., 2008). Seep carbonates comprise authigenic carbonate phases including mainly aragonite and minor calcite and dolomite cements. The authigenic carbonate minerals cement seafloor sediments, ranging from cm-sized cemented nodules to meter-sized mounds and exhaustive seafloor pavements (e.g., Greinert et al., 2001; Teichert et al., 2003; Naehr et al., 2007; Himmler et al., 2015; Sauer et al., 2017; Crémière et al., 2018). By using uranium–thorium (U–Th) radioisotopic dating of seep carbonates, the chronology of methane flux episodes can be reconstructed, which plausibly reflects the timing of various environmental and geological mechanisms triggering past methane release (e.g., Teichert et al., 2003; Feng et al., 2010; Crémiere et al., 2016; Himmler et al., 2019).

On the formerly glaciated Barents Sea shelf more than 7000 active hydrocarbon seeps have been discovered, originating from Palaeozoic through Cenozoic petroleum systems (e.g., Serov et al., 2023; Thorsnes et al., 2023). Upward gas migration is controlled by multiple geological mechanisms, including faults/fractures connecting reservoirs to the seafloor, reservoir rocks structurally exposed at the seafloor, and repeated glacial erosion of cap rocks (e.g., Andreassen et al., 2017; Serov et al., 2023). Depending on the ambient pressure–temperature conditions, rising methane may be sequestered as or released from gas hydrate in the shallow sub-seafloor gas hydrate stability zone (GHSZ; e.g., Chand et al., 2008; Andreassen et al., 2017). While the GHSZ was relatively thicker when grounded ice sheets covered the Barents Sea during the Last Glacial Maximum (LGM; ≈20,000 ka), oceanographic and environmental changes in concert with post–LGM ice retreat caused thinning of the hydrate stability zone, resulting in enhanced gas efflux (e.g., Andreassen et al., 2017; Serov et al., 2023). Indeed, hydrate-related enhanced post–LGM methane seepage has been suggested for various Barents Sea sites. It was previously put forward that increased bottom water temperatures in concert with depressurization and isostatic adjustment following the ice retreat has induced gas hydrate dissociation, resulting in strong episodic methane seepage in the south-west Barents Sea (Crémière et al., 2016). Likewise, ice-sheet and GHSZ modeling implies that the gradual changes in oceanographic conditions and isostatic adjustment following ice retreat promoted rapid gas hydrate dissociation and enhanced gas seepage in the north-west and central Barents Sea (Andreassen et al., 2017; Waage et al., 2019; Waage et al., 2020; Serov, et al., 2023). Regardless of the more than 7000 currently active hydrocarbon seeps mapped in the Barents Sea, seepage histories based on U–Th dates of seep carbonates corroborating enhanced post-glacial methane seepage have only been reported from the south-west Barents Sea (Crémière et al., 2016; Crémière et al., 2018; Argentino et al., 2022). Reconstruction of the post-glacial gas efflux chronology in the north-west and central areas of the Barents Sea has remained model-based to date.

Here we report petrographic and geochemical data including new U–Th dates of 17 seep carbonates collected from three active methane seeps located in the north-west (Storfjordrenna), central-north (Storbanken High), and south-west (Loppa High) Barents Sea (Figure 1). The U–Th dates reveal multiple episodes of seep carbonate precipitation and enhanced methane release since the late Pleistocene through the Holocene. The new carbonate ages are in agreement with strong episodic gas efflux in the Barents Sea following ice-retreat, and allow us to reconstruct the seepage chronology and associated carbonate formation after deglaciation.

2 Materials and methods

Seep carbonates were sampled from the seabed using remotely operated vehicles (ROVs) during four expeditions (Table 1; Figure 1); samples HH1029 and HH1077 were collected using the ROV 30K (Centre for Autonomous Marine Operations and Systems AMOS, Norwegian University of Science and Technology) during expedition CAGE16–5 with R/V Helmer Hanssen in 2016; the other samples were retrieved with the ROV Ægir 6000 (University of Bergen) during R/V Kronprins Haakon expedition CAGE18–5 in 2018 (Bünz et al., 2022); the PR1810 and PL954 samples were collected using a work class ROV (FMC Technologies) during two expeditions with M/S Bourbon Arctic in 2018.

2.1 XRD analyses

Quantitative mineralogical compositions were determined by powder X-ray diffraction and are reported in weight-% (wt%; Table 2). Powders were produced by pulverizing broken chunks (i.e., bulk-rock) and micro-drilling of cut slabs using a hand-held micro-drill. The powders were analysed with a Bruker D8 Advance diffractometer using Cu K α radiation at a 2Θ scanning angle of 3°–75° (step size of 0.02°, 1 s per step). Minerals were identified by automatic and manual peak search using the Bruker DIFFRAC EVA3.1 software; quantification was performed applying Rietveld refinement with the TOPAS 5 software. Repeated internal standard measurements yielded a detection limit and uncertainty of ±2 wt%.

2.2 Petrography and carbonate $\delta^{13}C$ and $\delta^{18}O$ analyses

Thin sections (6.5 x 5 cm) were prepared from ca. 1.5 cm thick cut slabs that were embedded in epoxy resin. The thin sections were examined using standard petrographic microscopy (Figure 2). Samples for stable carbon and oxygen isotopes ($\delta^{13}C$ and $\delta^{18}O$) were drilled from the surface of cut slabs with a hand-held micro-drill. Approximately 200 µg of the obtained powders were reacted with anhydrous phosphoric acid in a GasBench II preparation line; released CO_2 gas was analysed with a ThermoScientific Delta V Advantage isotope ratio mass spectrometer. The $\delta^{13}C$ and $\delta^{18}O$ values are reported in per mill (‰) relative to the Vienna–Pee Dee Belemnite standard (V–PDB). The data were calibrated against standard materials and the uncertainties for $\delta^{13}C$ and $\delta^{18}O$ were not higher than ± 0.2‰.

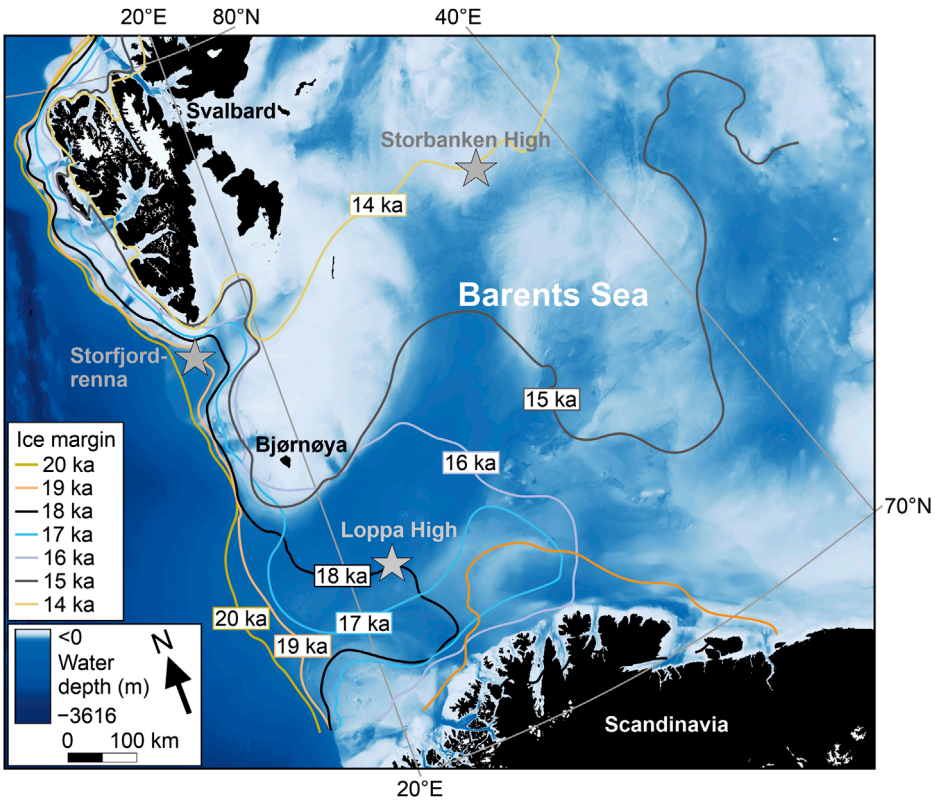

FIGURE 1
Sampling locations (stars) in the north-west (Storfjordrenna), central-north (Storbanken High), and south-west (Loppa High) Barents Sea, relative to reconstructed marine-based ice margin positions during deglaciation (redrawn after Sejrup et al., 2022; bathymetry data from Jakobsson et al., 2012).

2.3 Uranium–thorium dating

From 17 seep carbonates the U–Th ages of 55 fibrous cement samples were determined. Sample powders between 0.2 and 9.3 mg were obtained from polished cut slabs using a hand-held micro-drill. After powder digestion in 8 M HNO_3 U and Th were separated, concentrated, and analysed as described previously (Crémière et al., 2016). In brief, after digestion, centrifuging, and detritus dissolution, U and Th were pre-concentrated by iron co-precipitation and separated via column ion chromatography (Edwards et al., 1987). Isotope ratios were measured with a Neptune Plus multicollector inductively coupled plasma mass spectrometer. Argon and nitrogen were used as carrying gases to minimize oxide formation. Uranium–Th ages were calculated using an in-house spreadsheet, applying the ^{230}Th and ^{234}U decay constants of Cheng et al. (2013). Initial ^{230}Th correction was based on mean continental crust values. Sample ages are given in thousand years before present (ka BP; BP = before 1950). Samples with ^{230}Th/^{232}Th activity ratios ≤2 were rejected for data interpretation. The initial U isotope signature of seep carbonate tends to reflect seawater values or slight enrichment in ^{234}U relative to seawater if precipitation occurs under more restrictive conditions from pore fluids (Teichert et al., 2003). Therefore, analyses where $(^{234}U/^{238}U)_i$ sample <1.14 or $(^{234}U/^{238}U)_i$ sample >1.18 were assumed to represent an open-system behaviour with respect to U and/or Th, and were rejected for interpretation, too (see Supplementary Figure S1).

3 Results

3.1 Mineralogy, petrography, and carbonate $\delta^{13}C$ and $\delta^{18}O$ values

Aragonite is the main carbonate mineral (22–90 wt%), followed by moderate to low contents in magnesium-calcite (Mg-calcite; 3 to 63 wt%) and calcite (up to 22 wt%; Table 2). Quartz, feldspar, and clay minerals are the major non-carbonate components, ranging between 3 and 17 wt%. Micro-drilled fibrous aragonite in samples HH1029 and HH1077 is completely devoid of non-carbonate components (Table 2). Micrite in sample HH1029 has more Mg-calcite (63 wt%) than aragonite (22 wt%), whereas micrite in HH1077 is mainly aragonite (77 wt%) with only trace Mg-calcite content (below 2 wt%).

The carbonates comprise porous intraformational breccias of micrite-cemented sediment clasts, cemented by fibrous aragonite crusts (Figure 2; Supplementary Figures S1–S6). Relatively earlier formed micrite cemented clasts and subsequently formed fibrous aragonite cement comprise the volumetric dominant microfacies. The micrite cements hemipelagic sediment rich in silt-sized quartz and feldspar grains (Figures 2A,D). Fibrous aragonite forms mm-to cm-thick cement crusts, partly surrounding clasts and filling the pore space between micrite-cemented sediment and bioclasts (Figures 2B, C; Supplementary Figures S1–S6). Samples from Storfjordrenna show abundant tube-worm fossils in

10.3389/feart.2024.1355621

TABLE 1 Overview of sampling sites and locations; GHP = gas hydrate pingo; mbsl = meters below sea level.

Sample	Location	Site	Latitude [N]	Longitude [E]	Water depth (mbsl)
HH1029	NW Barents Sea	Storfjordrenna, GHP 3	76°6′24.804″	15°58′4.728″	378
HH1077	NW Barents Sea	Storfjordrenna, GHP 3	76°6′25.2″	15°58′9.876″	378
CAGE18–5–C1	NW Barents Sea	Storfjordrenna, GHP 3	76°6′25.204″	15°58′4.195″'	377
CAGE18–5–C2	NW Barents Sea	Storfjordrenna, GHP 3	76°6′25.628″	15°58′7.372″	378
CAGE18–5–C3	NW Barents Sea	Storfjordrenna, GHP 3	76°6′25.585″	15°58′7.813″	379
CAGE18–5–C4	NW Barents Sea	Storfjordrenna, GHP 3	76°6′25.799″	15°58′7.79″	379
CAGE18–5–C5	NW Barents Sea	Storfjordrenna, GHP 3	76°6′25.75″	15°58′7.669″	379
CAGE18–5–C6	NW Barents Sea	Storfjordrenna, GHP 3	76°6′25.198″	15°58′0.101″	379
CAGE18–5–C7	NW Barents Sea	Storfjordrenna, GHP 3	76°6′25.297″	15°57′59.961″	379
CAGE18–5–C11	Central-north Barents Sea	Storbanken High	76°46′49.007″	35°9′45.99″	156
CAGE18–5–C14	Central-north Barents Sea	Storbanken High	76°46′56.926″	35°13′51.4″	158
PR 1810–001	SW Barents Sea	Loppa High	72°4′2.442″	21°48′19.3356″	383
PR 1810–002	SW Barents Sea	Loppa High	72°4′2.365″	21°48′19.3608″	382
PR 1810–003	SW Barents Sea	Loppa High	72°4′2.481″	21°48′19.4832″	383
PR 1810–051	SW Barents Sea	Loppa High	72°4′2.524″	21°48′20.1024″	383
PL954–C1	SW Barents Sea	Loppa High	71°57′58.104″	21°35′11.256″	354
PL954–C2	SW Barents Sea	Loppa High	71°57′58.104″	21°35′11.256″	354

both, micrite and fibrous cement (Figures 2A, B), relatively few articulated bivalve shells, and centimetre-sized grains of ice-rafted debris (IRD; Supplementary Figures S1–S3). Likewise, the Storbanken High samples display some bivalve shells and IRD grains (Supplementary Figures S3D, E). Samples from the Loppa High contain many articulated bivalves with abundant inter- and intraparticle fibrous cement (Supplementary Figure S5). Macroscopically, fibrous cement in the Loppa High samples can be distinguished into whitish and grey aragonite. Whitish aragonite appears as incoherent layer of inclusion-rich, cryptocrystalline cement between micrite and fibrous aragonite (Figure 2E; Supplementary Figures S6). Under UV light cryptocrystalline aragonite exhibits intense fluorescence, whereas subsequent clear fibrous aragonite is non-fluorescent. Likewise, dark inclusion-rich clotted aragonite and brownish botryoidal aragonite display strong fluorescence (Figure 2F). Occasionally, pockets of a few square centimetre size containing cemented IRD are intercalated within cemented clasts and bivalves (Supplementary Figures S6).

Carbonate $\delta^{13}C$ and $\delta^{18}O$ values were analysed for micrite (n = 47) and fibrous cement (n = 47; Figure 3; Supplementary Figures S1). Overall, $\delta^{13}C$ values range from −43.3 to −18.4‰ while the $\delta^{18}O$ values range from 3.1‰ to 5.6‰. Micrite yielded slightly lower $\delta^{13}C$ (median ±SD: −32.2‰ ± 4.8‰) and slightly higher $\delta^{18}O$ (4.8‰ ± 0.5‰) values than fibrous cement ($\delta^{13}C$ = −31.2‰ ± 5.1‰; $\delta^{18}O$ = 4.6‰ ± 0.5‰). Samples from Storbanken High exhibit relatively lower $\delta^{13}C$ values (−37.8‰ ± 3.7‰; n = 19) than the Loppa High (−31.9‰ ± 3.6‰; n = 51) and Storfjordrenna (−27.0‰ ± 2.5‰; n= 30) samples. Storfjordrenna samples show relatively higher $\delta^{18}O$ values (5.0‰ ± 0.3‰) than the samples from Storbanken (4.9‰ ± 0.2‰) and Loppa High (4.3‰ ± 0.5‰).

3.2 Carbonate U–Th ages

From the 55 micro-drilled U–Th samples, four have been discarded for interpretation due to relatively low data quality and resulting high uncertainty, and three are coral skeleton material (Figure 4; Supplementary Figure S1–S6; Supplementary Figure S1). Samples C1 through C7, HH1029, and HH1077, were collected from the gas hydrate pingo mound 3 (GHP 3; Serov et al., 2017) at Storfjordrenna and yielded exclusively mid to late Holocene ages, ranging from 6.3 ± 2.3 (ka ± 2σ) to 1.2 ± 0.1 ka. The two samples from the Storbanken High area yielded one late Pleistocene 13.5 ± 2.4 ka (one subsample from C11) and three mid-Holocene ages from 6.6 ± 0.3 to 5.4 ± 0.1 ka (three subsamples, C14). Samples PR1810 and PL954 from the Loppa High area exhibit late Pleistocene and early to mid Holocene ages, ranging from 13.4 ± 0.7 to 4.1 ± 1.3 ka. The three coral samples exhibit Holocene ages from 10.4 ± 1.3 to 4.2 ± 1.3 ka.

TABLE 2 Mineralogical compositions (weight−%). Arag = aragonite; Cc = calcite Mg-Cc = magnesium calcite; Qtz = quartz; K-fsp = potassium feldspar; Plc = plagioclase; Clays = illite, muscovite, smectite, and chlorite; tr. = trace; n.d. = not detected.

Sample	Site	Sampling method	Microfacies	Arag	Cc	Mg-Cc	Qtz	K-fsp	Plc	Clays
HH1029	Storfjordrenna, GHP 3	micro-drill	micrite	22	n.d	63	10	n.d	tr	5
HH1029	Storfjordrenna, GHP 3	micro-drill	fibrous cement	78	22	n.d	n.d	n.d	n.d	n.d
HH1077	Storfjordrenna, GHP 3	micro-drill	fibrous cement	90	10	n.d	n.d	n.d	n.d	n.d
HH1077	Storfjordrenna, GHP 3	micro-drill	micrite	77	tr.	3	11	n.d	4	4
CAGE18–5–C1	Storfjordrenna, GHP 3	broken chunk	bulk-rock	43	n.d	31	10	n.d	4	12
CAGE18–5–C2	Storfjordrenna, GHP 3	broken chunk	bulk-rock	55	n.d	15	11	n.d	4	14
CAGE18–5–C3	Storfjordrenna, GHP 3	broken chunk	bulk-rock	68	n.d	8	10	n.d	4	10
CAGE18–5–C4	Storfjordrenna, GHP 3	broken chunk	bulk-rock	71	n.d	7	9	n.d	3	10
CAGE18–5–C5	Storfjordrenna, GHP 3	broken chunk	bulk-rock	65	n.d	10	9	n.d	4	12
CAGE18–5–C6	Storfjordrenna, GHP 3	broken chunk	bulk-rock	80	n.d	5	4	n.d	3	8
CAGE18–5–C7	Storfjordrenna, GHP 3	broken chunk	bulk-rock	61	n.d	17	8	n.d	3	11
CAGE18–5–C11	Storbanken High	broken chunk	bulk-rock	40	n.d	28	11	3	6	12
CAGE18–5–C14	Storbanken High	broken chunk	bulk-rock	61	n.d	7	17	3	4	8
P1810–001–5	Loppa High	broken chunk	bulk-rock	68	n.d	9	8	n.d	4	11
P1810–002–2	Loppa High	broken chunk	bulk-rock	61	n.d	23	5	n.d	3	8
P1810–003–2	Loppa High	broken chunk	bulk-rock	70	n.d	3	8	n.d	5	14
P1810–051–2	Loppa High	broken chunk	bulk-rock	66	n.d	4	14	3	5	8

4 Discussion

4.1 Carbonate precipitation induced by anaerobic oxidation of methane and non-methane hydrocarbons

The carbonate $\delta^{13}C$ values are as low as previously reported values of seep carbonates sampled from the south-west and north-west Barents Sea (Crémière et al., 2016; Crémière et al., 2018; Yao et al., 2021; Argentino et al., 2022), and indicate a predominantly hydrocarbon-derived carbon source. Seepage gas samples from Storfjordrenna and Loppa High show a thermogenic composition and yielded $\delta^{13}C_{methane}$ values of −47‰ and−48% V–PDB, respectively (Crémière et al., 2016; Serov et al., 2017). Weniger et al. (2019) extracted gas from surface sediments at Storfjordrenna and report a thermogenic composition with slightly higher average $\delta^{13}C_{methane}$ of −41.3‰ ± 2.7‰ V–PDB (n=4). In the same study, Weniger et al. (2019) show a thermogenic gas composition with average $\delta^{13}C_{methane}$ of −50.8‰ ± 5.2‰ V–PDB (n=18) for surface sediment bound gas from the Olga Basin, which borders along the southern flank of the Storbanken High. To the best of the authors' knowledge there are no published methane $\delta^{13}C$ values for seepage or bound gas from the Storbanken High seeps. Given that the Storbanken High and the Olga Basin share the same reservoir rocks (Lundschien et al., 2023; Serov et al., 2023), a thermogenic origin for the gas seeping at Storbanken High is assumed.

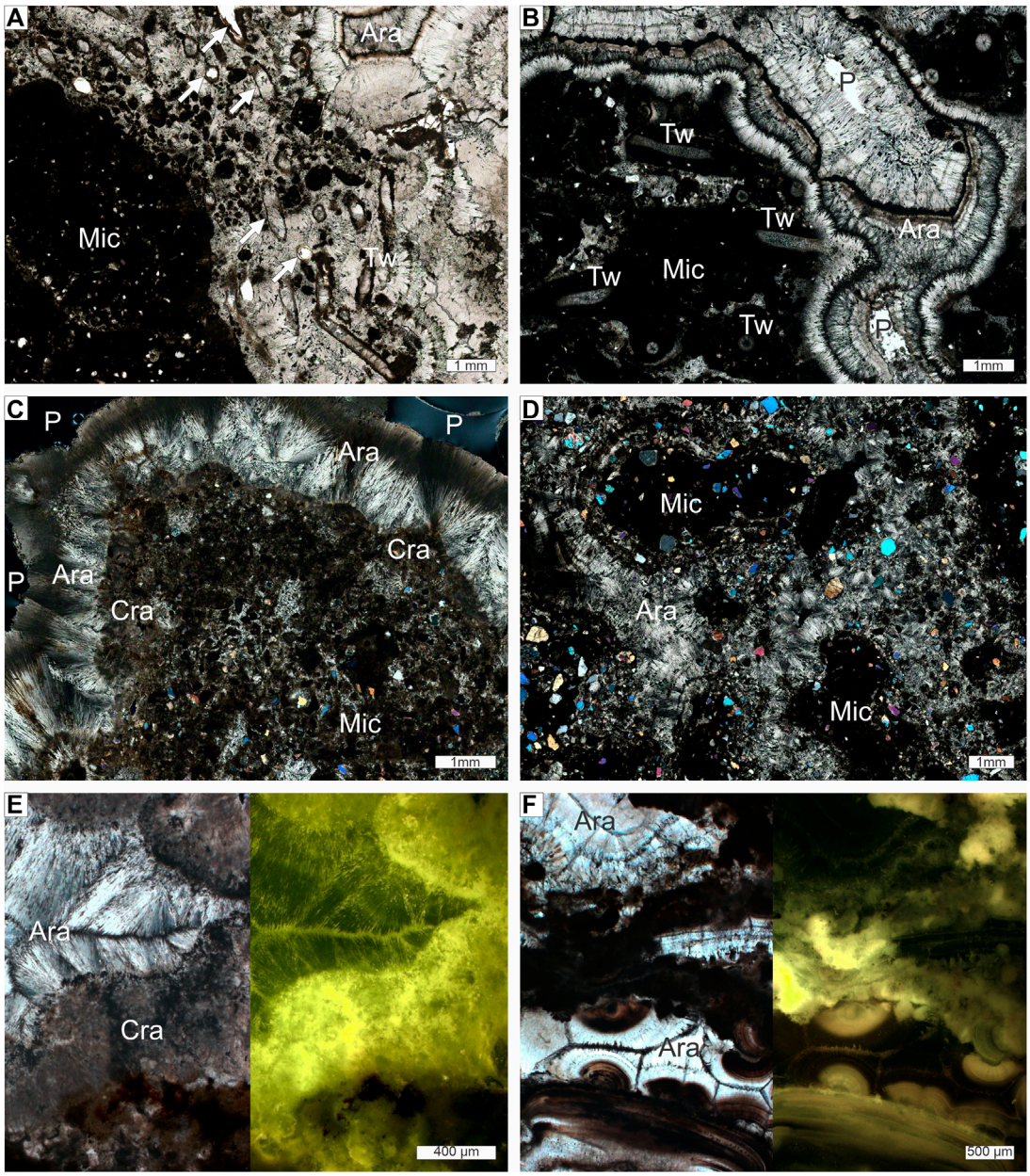

FIGURE 2
Thin section micrographs of representative seep carbonates from Storfjordrenna **(A,B)**, Storbanken High **(C,D)**, and Loppa High **(E,F)**; PPL = parallel-polarized light, XPL = cross-polarized light; P = pore space. **(A)** Sample CAGE18-5-C1, showing micrite-cemented sediment (Mic) with abundant silt-sized quartz grains, surrounded by radial and botryoidal aragonite (Ara) cement; please note the abundant dark layered, and clotted and peloidal inclusions; note also the longitudinal/oblique and perpendicular cut tube worm walls (Tw; arrows) which are open or completely cemented; Tw are likely fossils of siboglinid *Oligobrachia* sp. (Sen et al., 2018); PPL, open pore space appears white. **(B)** Sample CAGE18-5-C4 with abundant cemented tubes in micritic sediment (Mic), cross-cut by multiple layers of dark inclusion rich, mm-thick radial and botryoidal aragonite (Ara); PPL. **(C)** XPL view (pore space appears black) of sample CAGE18-5-C11, showing micrite-cemented sediment with silt-sized quartz and some areas with clotted micrite, surrounded by botryoidal aragonite (Ara); note that the aragonite fans originate from a layer of inclusion-rich cryptocrystalline aragonite (Cra). **(D)** Sample CAGE18-5-C14 exhibiting rounded clasts of micrite-cemented sediment (Mic), cemented by radial fibrous aragonite (Ara); note abundant siliciclastic grains cemented fibrous aragonite (XPL). **(E)** and **(F)** show transmitted light (left panels, XPL) and UV epifluorescence images (right panels) of samples PR 1810–002 and PL954-02, respectively; inclusion-rich cryptocrystalline aragonite (Cra) and clotted and botryoidal aragonite in sample P1810-002; note the stronger fluorescence of Cra compared to clear non-fluorescent aragonite; inclusion-rich clotted and botryoidal aragonite (Ara) in sample PL954-02 exhibits strong fluorescence whereas clear aragonite is non-fluorescent.

The seep carbonates are relatively ^{13}C-enriched compared to the methane. This is interpreted as the result of mixing ^{13}C-depleted dissolved inorganic carbon (DIC) with ^{13}C-rich DIC during carbonate precipitation, yielding higher carbonate δ^{13}C values relative to the parent methane (Formolo et al., 2004; Peckmann and Thiel, 2004; Roberts et al., 2010; Himmler et al., 2015). Seep carbonate δ^{13}C values represent a DIC mixture of seawater (δ^{13}C ≈ 0‰), DIC produced during organiclastic sulfate

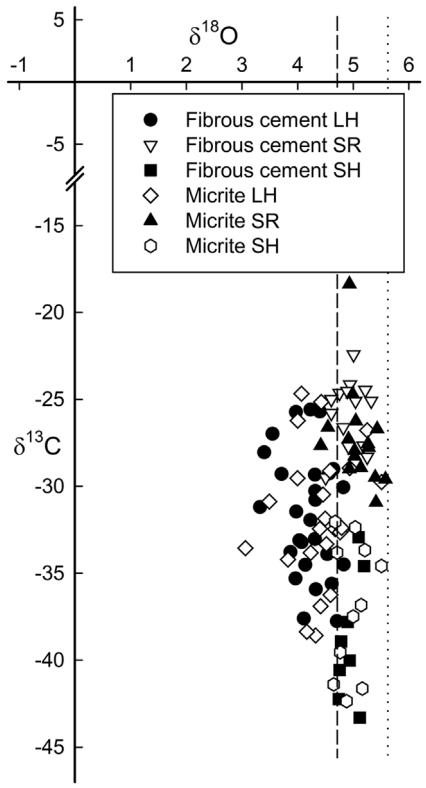

FIGURE 3
Seep carbonate $\delta^{13}C$ and $\delta^{18}O$ values (‰ V–PDB); LH = Loppa High, SR = Storfjordrenna; SH = Storbanken High. The dashed and stippled lines mark theoretical $\delta^{18}O$ values for aragonite (4.7‰) and magnesium-calcite (5.6‰) precipitated in equilibrium with bottom water at 1°C temperature and $\delta^{18}O$ = 1‰ (Vienna–Standard Mean Ocean Water) assumed for ≈15 ka (see Crémière et al., 2016).

reduction (≈ −25‰), and DIC produced by AOM/or and oxidation of higher hydrocarbons ($\delta^{13}C$ below −20‰; e.g., Irwin, et al., 1977; Formolo et al., 2004; Sassen et al., 2004; Smrzka et al., 2019). Whereas the highest $\delta^{13}C_{carbonate}$ value of −18‰ (Figure 3; Supplementary Figure S1) can be explained by a DIC mixture of seawater and organiclastic sulfate-reduction, the rest of the $\delta^{13}C_{carbonate}$ values between −43‰ and −24‰ point to a DIC mixture produced by the anaerobic oxidation of the thermogenic methane and/or non-methane hydrocarbons (Formolo et al., 2004; Sassen et al., 2004; Smrzka et al., 2019). The relatively lower values indicate a higher contribution of AOM-derived DIC, whereas the relatively higher values indicate significant contribution DIC resulting from the anaerobic oxidation non-methane hydrocarbons (Formolo et al., 2004).

Aragonite is the dominant carbonate phase, except for the magnesium-calcite rich micrite in sample HH1029 (Table 2). It is not unusual for seep carbonates to mainly comprise aragonite and partly include Mg-calcite (e.g., Greinert et al., 2001; Crémière et al., 2018; Lu et al., 2021). At hydrocarbon seeps aragonite formation is likely favoured over calcite by relatively high sulfate concentrations (Burton, 1993). Bioturbation of the sediment by bivalves and bubble ebullition during episodes of strong gas efflux likely eased entrainment of sulfate-rich seawater into the shallow subsurface, supporting sulfate-driven AOM near the sediment–water interface (e.g., Borowski et al., 1999; Aloisi et al., 2002; Luff et al., 2004). In contrast, during episodes of weak seepage with low gas flux, AOM was likely mediated deeper in the sediment at relatively lower pore water sulfate concentrations, and Mg-calcite precipitation was favoured (e.g., Greinert et al., 2001). Increased magnesium incorporation into the calcite lattice is plausible under low flux conditions, when abundant AOM-produced hydrogen sulfide (HS^-) supports de-hydration of Mg^{2+} ions, thus increasing the pore fluid Mg^{2+}/Ca^{2+} ratio (Zhang et al., 2012; Lu et al., 2021). At the same time, the increased alkalinity resulting from AOM-produced bicarbonate (HCO_3^-) also supports carbonate precipitation.

Overall, the aragonite-dominated mineralogy is congruent with carbonate precipitation near the sediment–water interface. This is also supported by the macrofossil content, including the chemosynthesis-based siboglinid tube worms *Oligobrachia* sp. (Sen et al., 2018; Åström et al., 2018), unidentified articulated bivalves, and a presumably cool water coral (Figure 2, Supplementary Figures S1–S6). Moreover, molecular fossils including ^{13}C-depleted lipid biomarkers diagnostic of AOM-mediating methanotrophic archaea and sulfate-reducing bacteria have been found in Storfjordrenna samples HH1029 and HH1077, corroborating that microbial-mediated sulfate-driven AOM induced carbonate precipitation (Yao et al., 2021). Although no lipid biomarker data are available for the Storbanken High and Loppa High samples, they contain abundant microbial textures, including clotted micrite and cryptocrystalline aragonite (Figures 2C–F; Riding, 2000; Zwicker et al., 2018). Both textures exhibit strong fluorescence under UV radiation, indicative of high organic matter content resulting from *in situ* organomineralization (Neuweiler et al., 2000). Given that increased carbonate alkalinity at methane seeps supports the lithification of microbial biofilms, it is feasible that the fluorescent textures observed in the Storbanken High and Loppa High samples represent mineralized AOM hotspots (Himmler et al., 2018; Zwicker et al., 2018). Remarkably, the strong fluorescent textures in samples PR1810-002 and PL945-C2 (Figures 2E,F) correspond macroscopically to whitish aragonite, similar to whitish and cryptorcrystalline aragonite with high AOM-biomarker contents described in modern and ancient seep carbonates (Leefmann et al., 2008; Hagemann et al., 2013).

4.2 Timing of seep-carbonate formation relative to the palaeoenvironment

Regarding the reconstructed ice margins, all U–Th dates are consistent with carbonate formation after local ice retreat and protracted methane flux (e.g., Crémière et al., 2016; Serov et al., 2023). The oldest samples C11 (Storbanken High; SH) and PR1810-001C (Loppa High; LH) yielded similar ages of 13.5 (SH) and 13.4 (LH) ka. The ages indicate relatively high gas flux and associated seep carbonate formation at these two distant sites during the Bølling–Allerød interstadial. At this time, influx of relatively warmer Atlantic seawater promoted rapid disintegration of the grounded Barents Sea ice sheet, leaving large areas in the west and south-west Barents Sea ice free (e.g., Rasmussen and Thomsen, 2021; Sejrup et al., 2022). The influx of warm water likely accelerated the dissociation of shallow subsurface gas hydrates, resulting in

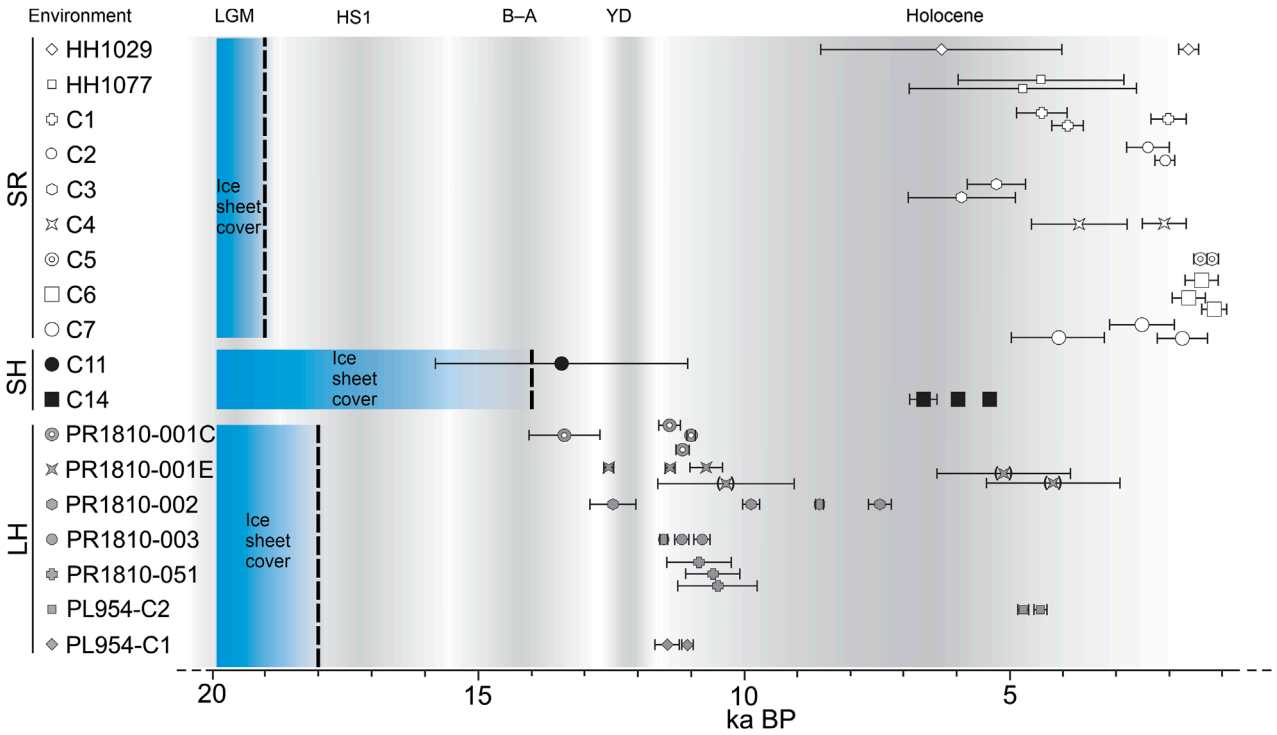

FIGURE 4
Seep carbonate U–Th ages (±2σ) from Storfjordrenna (SR), Storbanken High (SH) and Loppa High (LH), relative to reconstructed regional ice cover and palaeoenvironment (vertical shaded bars). Symbols in brackets indicate coral skeleton ages (seep carbonate sample PR 1810–001E; note that the oldest coral date is likely a mixture of skeleton and seep carbonate cement); HS1 = Heinrich stadial 1 (cool); B–A = Bølling–Allerød interstadial (warm); YD, Younger Dryas (cool); palaeoenvironment timing after Rasmussen and Thomsen (2021); ice-sheet cover after Sejrup et al. (2022).

increased methane emissions at the seafloor (Crémière et al., 2016; Andreassen, et al., 2017). This is congruent with the SH carbonate $\delta^{18}O$ values, indicating a contribution of hydrate-derived ^{18}O-enriched water during carbonate precipitation (Figure 3).

Except for sample PL954–C2 (≈4.7 and 4.4 ka), the rest of the non-coral LH samples have late Pleistocene and early Holocene U–Th ages between ≈12.6 and 7.5 ka. Overall, the LH dates are in agreement with previously reported seep carbonate U–Th dates from the south-west Barents Sea and northern Norwegian Sea, together indicating episodic post–LGM hydrocarbon gas release and seep carbonate formation between 17.5 and 1.6 ka (Crémière et al., 2016; Sauer et al., 2017; Crémière et al., 2018; Argentino et al., 2022). Sauer et al. (2017) suggested that in northern Scandinavia, seismic activities and resulting fault reactivation and changes in reservoirs pore pressure could have triggered gas seepage around ≈11 and 4 ka. Remarkably, the majority of the new LH U–Th ages between 12 and 10 ka plus the two ages of sample PL954–C2 (≈4.7 and 4.4 ka), are in agreement with this scenario.

The carbonate ages reveal lag times between local ice retreat and distinct episodes of enhanced gas efflux. It needs to be stressed that the reported ages were exclusively derived from relatively late-stage fibrous aragonite cement and do not constrain the initial seepage stage (see also Crémière et al., 2016; Crémière et al., 2018). In particular at Storfjordrenna, seep carbonate formation occurred ≈13 ka after the grounded ice has had retreated after ≈19 ka (Rasmussen and Thomsen, 2021; Sejrup et al., 2022). The long lag time at Storfjordrenna is surprising, considering that abundant gas hydrates (and probably free gas) had accumulated in the subsurface during the LGM in an approximately 200 m thick GHSZ (Serov et al., 2017). After glacial retreat, the GHSZ totally diminished by ≈13 ka and must have released significant gas amounts from the seabed due to gas hydrate dissociation (Serov et al., 2017). Yet, the carbonate ages do not indicate carbonate formation before 6.3 ka. It could be that the U–Th ages of seafloor-sampled seep carbonates do not reflect the entire post–LGM seepage history, and large ice bergs from the disintegrating ice sheet might have eroded any older seep carbonates from the seafloor (Rasmussen and Thomsen, 2021). El bani Altuna et al. (2021) showed that the average bottom water temperature at Storfjordrenna increased from 2.5°C ± 1°C to 4.3°C ± 1°C between ≈13 and 5 ka, followed by cooling down to down 2.8°C ± 1°C after 4 ka. In addition, their gas hydrate model suggests that a fluctuating GHSZ existed between 13 and 9 ka (i.e., variable thickness of 0 to ca. 100 m below seafloor), but was absent between 9 and 5 ka, resulting in liberation of gas and hydrate-derived water. Remarkably, the gas hydrate modeling also shows a stable GHSZ since 5 ka, which would sequester most of the upward migrating gas. Yet, our U–Th ages show constant seep carbonate formation near the sediment–water interface since 6.3 ka. Regardless of the existence of the GHSZ, the carbonate dates support the notion that the underlying hydrocarbon reservoir actively injects thermogenic methane into the shallow subsurface sediments at this site, probably since the mid to late Holocene until modern times, as put forward by Waage et al. (2019). Given constant gas supply from below and the resulting high methane concentrations, free methane likely

bypasses the GHSZ through cracks and faults, eventually escaping at the seafloor.

Seep carbonate $\delta^{18}O$ values depend on the mineralogy, the ambient temperature and the $\delta^{18}O$ of the carbonate-precipitating fluid, and serve as proxy for possible gas hydrate dissociation during carbonate formation (e.g., Aloisi et al., 2000; Greinert et al., 2001; Crémière et al., 2016; Crémière et al., 2018). Assuming seep carbonate formation under post-glacial conditions, i.e., bottom water temperature 1°C and seawater $\delta^{18}O$ = 1‰ V–SMOW (Duplessy et al., 2002), carbonate $\delta^{18}O$ values of 4.7‰ for aragonite and 5.6‰ for magnesium–calcite would be expected (Kim et al., 2007; Crémière et al., 2016). Samples from Storfjordrenna (median $\delta^{18}O$ = 5.0) and Storbanken High (median $\delta^{18}O$ = 4.9) show carbonate $\delta^{18}O$ values slightly higher than 4.7‰, while the Loppa High samples are mostly (but not exclusively) below 4.7‰ (median $\delta^{18}O$ = 4.3; Figure 3). Values above 4.7‰ would indicate either precipitation from fluids below 1°C temperature or relatively enriched in ^{18}O, while lower values point to precipitation at slightly higher temperatures or fluids depleted in ^{18}O. Given that the reconstructed bottom water temperature was above 2°C in the Storfjordrenna since the early Holocene (El bani Altuna et al., 2021; Rasmussen and Thomsen, 2021), the seep carbonates most likely precipitated from ^{18}O-enriched fluids. It is feasible that the ^{18}O-rich fluids originated from extensive post–LGM gas hydrate dissociation, since hydrate incorporates preferentially ^{18}O (Davidson et al., 1983; Serov et al., 2023). Considering that warm water influx has triggered abrupt gas hydrate dissociation to form large craters on the seafloor between 15 and 12 ka ago (Andreassen et al., 2017), a similar formation scenario for the ≈6 ka old Storbanken High sample C14 is suggested. Influx of warmer bottom water around 6 ka, as shown by El bani Altuna et al. (2021), likely accelerated gas hydrate dissociation in the shallow subsurface, which would explain the relatively ^{18}O-erniched carbonates. For the Loppa High samples, most of the carbonate $\delta^{18}O$ values can be explained by precipitation in equilibrium with ambient post–LGM bottom water temperatures. However, as pointed out by Crémière et al. (2018), a contribution of ^{18}O-rich fluids from the relatively deeper reservoir and/or from gas hydrate dissociation can not be ruled out, considering the complex tectono–sedimentary history and possible fluid dilution effects during carbonate precipitation.

5 Conclusions

1) Carbonates sampled from active gas seeps at Storfjordrenna, Storbanken High, and Loppa High areas in the Barents Sea formed as a result of the anaerobic oxidation of methane and higher hydrocarbons. New U–Th ages overlap with previously published ages for seep carbonates from the south-west Barents Sea, corroborating episodic gas release and carbonate precipitation in the aftermath of the retreat of the Barents Sea–Svalbard Ice Sheet since the Last Glacial Maximum.
2) Major carbonate formation periods occurred after the Bølling–Allerød interstadial, during the Younger Dryas stadial, and at the beginning of and throughout the mid to late Holocene.
3) The U–Th ages from Storfjordrenna, where gas hydrates are present today, indicate seep carbonate precipitation resulting from gas hydrate dissociation-related methane release ca.13 ka after the marine-based ice sheet had retreated. The new U–Th ages indicate that carbonate formation continued between 6.3 and 1.2 ka.
4) At gas seeps which are structurally connected to deep-seated hydrocarbon reservoirs at Storbanken High and Loppa High, seep carbonates formed relatively early after the local ice retreat, indicating episodic gas release from ca.13.5 to 4.4 ka. It is speculated that seismic activity resulting from post-glacial isostatic adjustment reactivated faults and triggered episodic gas seepage.
5) Relatively ^{18}O-enriched seep carbonates indicate gas hydrate dissociation related seepage due to relative warmer bottom waters since the mid Holocene at Storfjordrenna and Storbanken High.

Data availability statement

The original contributions presented in the study are included in the article/Supplementary Material, further inquiries can be directed to the corresponding author.

Author contributions

TH: Conceptualization, Writing–original draft, Investigation. DW: Investigation, Writing–review and editing. DS: Investigation, Methodology, Writing–review and editing. SV: Investigation, Writing–review and editing. SC: Investigation, Writing–review and editing. TM: Investigation, Writing–review and editing. KK: Investigation, Writing–review and editing. RM: Investigation, Writing–review and editing. GP: Investigation, Writing–review and editing. SB: Funding acquisition, Writing–review and editing. DC: Investigation, Writing–review and editing. JK: Funding acquisition, Writing–review and editing. AL: Funding acquisition, Investigation, Writing–review and editing.

Funding

The author(s) declare financial support was received for the research, authorship, and/or publication of this article. This study was supported by CAGE and the Research Council of Norway through its Centres of Excellence scheme (Grant No. 223259) and the Petromaks2 NORCRUST project (Grant No. 255150).

Acknowledgments

Professional support by the masters and the crews during seagoing expeditions on R/V Helmer Hannsen (CAGE16–5), R/V Kronprins Haakon (CAGE18–5), and M/S Bourbon Arctic, as well as the skilled work of the respective ROV teams, are greatly acknowledged. We thank J. Schönenberger (Geological Survey of Norway) for the XRD measurements. Thoughtful comments by the Editor and the two reviewers helped to improve the manuscript.

Conflict of interest

The authors declare that the research was conducted in the absence of any commercial or financial relationships that could be construed as a potential conflict of interest.

Publisher's note

All claims expressed in this article are solely those of the authors and do not necessarily represent those of their affiliated organizations, or those of the publisher, the editors and the reviewers. Any product that may be evaluated in this article, or claim that may be made by its manufacturer, is not guaranteed or endorsed by the publisher.

Supplementary material

The Supplementary Material for this article can be found online at: https://www.frontiersin.org/articles/10.3389/feart.2024.1355621/full#supplementary-material

References

Aloisi, G., Bouloubassi, I., Heijs, S. K., Pancost, R., Pierre, C., Sinninghe Damsté, J. S., et al. (2002). CH4-consuming microorganisms and the formation of carbonate crusts at cold seeps. *Earth Planet. Sci. Lett.* 203, 195–203. doi:10.1016/s0012-821x(02)00878-6

Aloisi, G., Pierre, C., Rouchy, J.-M., Foucher, J.-P., and Woodside, J. (2000). Methane-related authigenic carbonates of eastern Mediterranean Sea mud volcanoes and their possible relation to gas hydrate destabilisation. *Earth Planet Sci. Lett.* 184, 321–338. doi:10.1016/S0012-821X(00)00322-8

Andreassen, K., Hubbard, A., Winsborrow, M., Patton, H., Vadakkepuliyambatta, S., Plaza-Faverola, A., et al. (2017). Massive blow-out craters formed by hydrate controlled methane expulsion from the Arctic seafloor. *Science* 356 (80), 948–953. doi:10.1126/science.aal4500

Argentino, C., Lee, A., Fallati, L., Sahy, D., Birgel, D., Peckmann, J., et al. (2022). Biogeochemistry and timing of methane-derived carbonate formation at Leirdjupet fault complex, SW Barents sea. *Front. Earth Sci.* 10, 1029471. doi:10.3389/feart.2022.1029471

Åström, E. K. L., Carroll, M. L., Ambrose, W. G., Sen, A., Silyakova, A., and Carroll, J. (2018). Methane cold seeps as biological oases in the high-Arctic deep sea. *Limnol. Oceanogr.* 63, S209–S231. doi:10.1002/lno.10732

Beal, E. M., House, C. H., and Orphan, V. J. (2009). Manganese- and iron-dependent marine methane oxidation. *Science* 325, 184–187. doi:10.1126/science.1169984

Boetius, A., Ravenschlag, K., Schubert, C., Rickert, D., Widdel, F., Gieseke, A., et al. (2000). A marine microbial consortium apparently mediating anaerobic oxidation of methane. *Nature* 407, 623–626. doi:10.1038/35036572

Borowski, W. S., Paull, C. K., and Ussler, W. (1999). Global and local variations of interstitial sulfate gradients in deep-water, continental margin sediments: sensitivity to underlying methane and gas hydrates. *Mar. Geol.* 159, 131–154. doi:10.1016/S0025-3227(99)00004-3

Bünz, S., Vadakkepuliyambatta, S., Serov, P., Lepland, A., Himmler, T., Hong, W.-L., et al. (2022). CAGE18-5 Cruise report: remotely-operated vehicle (ROV) investigations of active gas seepage sites in the Barents Sea. *CAGE–Centre Arct. Gas Hydrate, Environ. Clim. Rep. Ser.* 6. doi:10.7557/cage.6853

Burton, E. A. (1993). Controls on marine carbonate cement mineralogy: review and reassessment. *Chem. Geol.* 105, 163–179. doi:10.1016/0009-2541(93)90124-2

Chand, S., Mienert, J., Andreassen, K., Knies, J., Plassen, L., and Fotland, B. (2008). Gas hydrate stability zone modelling in areas of salt tectonics and pockmarks of the Barents Sea suggests an active hydrocarbon venting system. *Mar. Petroleum Geol.* 25, 625–636. doi:10.1016/j.marpetgeo.2007.10.006

Cheng, H., Edwards, R. L., Shen, C.-C., Polyak, V. J., Asmerom, Y., Woodhead, J., et al. (2013). Improvements in 230Th dating, 230Th and 234U half-life values, and U–Th isotopic measurements by multi-collector inductively coupled plasma mass spectrometry. *Earth Planet. Sci. Lett.* 371, 82–91. doi:10.1016/j.epsl.2013.04.006

Crémière, A., Chand, S., Sahy, D., Thorsnes, T., Martma, T., Noble, S. R., et al. (2018). Structural controls on seepage of thermogenic and microbial methane since the last glacial maximum in the Harstad Basin, southwest Barents Sea. *Mar. Petroleum Geol.* 98, 569–581. doi:10.1016/j.marpetgeo.2018.07.010

Crémière, A., Lepland, A., Chand, S., Sahy, D., Condon, D. J., Noble, S. R., et al. (2016). Timescales of methane seepage on the Norwegian margin following collapse of the Scandinavian Ice Sheet. *Nat. Commun.* 7, 11509. doi:10.1038/ncomms11509

Davidson, D. W., Leaist, D. G., and Hesse, R. (1983). Oxygen-18 enrichment in the water of a clathrate hydrate. *Geochem. Cosmochim. Acta* 47, 2293–2295. doi:10.1016/0016-7037(83)90053-4

Duplessy, J.-C., Labeyrie, L., and Waelbroeck, C. (2002). Constraints on the ocean oxygen isotopic enrichment between the last glacial maximum and the Holocene: paleoceanographic implications. *Quat. Sci. Rev.* 21, 315–330. doi:10.1016/S0277-3791(01)00107-X

Edwards, R. L., Chen, J. H., and Wasserburg, G. J. (1987). 238U–234U–230Th–232Th systematics and the precise measurement of time over the past 500,000 years. *Earth Planet. Sci. Lett.* 81, 175–192. doi:10.1016/0012-821x(87)90154-3

Egger, M., Riedinger, N., Mogollón, J. M., and Jørgensen, B. B. (2018). Global diffusive fluxes of methane in marine sediments. *Nat. Geosci.* 11, 421–425. doi:10.1038/s41561-018-0122-8

El bani Altuna, N., Rasmussen, T. L., Ezat, M. M., Vadakkepuliyambatta, S., Groeneveld, J., and Greaves, M. (2021). Deglacial bottom water warming intensified Arctic methane seepage in the NW Barents Sea. *Commun. Earth Environ.* 2, 188. doi:10.1038/s43247-021-00264-x

Feng, D., Roberts, H. H., Cheng, H., Peckmann, J., Bohrmann, G., Edwards, R. L., et al. (2010). U/Th dating of cold-seep carbonates: an initial comparison. *Deep Sea Res. Part II* 57, 2055–2060. doi:10.1016/j.dsr2.2010.09.004

Formolo, H., Lyons, T. W., Zhang, C., Kelley, C., Sassen, R., Horita, J., et al. (2004). Quantifying carbon sources in the formation of authigenic carbonates at gas hydrate sites in the Gulf of Mexico. *Chem. Geol.* 205, 253–264. doi:10.1016/j.chemgeo.2003.12.021

Greinert, J., Bohrmann, G., and Suess, E. (2001). "Gas hydrate-associated carbonates and methane-venting at Hydrate Ridge: classification, distribution, and origin of authigenic lithologies," in *Natural gas hydrates: occurrence, distribution, and detection*. Editors C. K. Paull, and W. P. Dillon (Washington, DC, USA: American Geophysical Union).

Hagemann, A., Leefmann, T., Peckmann, J., Hoffmann, V.-E., and Thiel, V. (2013). Biomarkers from individual carbonate phases of an Oligocene cold-seep deposit, Washington State, USA. *Lethaia* 46, 7–18. doi:10.1111/j.1502-3931.2012.00316.x

Himmler, T., Birgel, D., Bayon, G., Pape, T., Ge, L., Bohrmann, G., et al. (2015). Formation of seep carbonates along the Makran convergent margin, northern Arabian Sea and a molecular and isotopic approach to constrain the carbon isotopic composition of parent methane. *Chem. Geol.* 415, 102–117. doi:10.1016/j.chemgeo.2015.09.016

Himmler, T., Sahy, D., Martma, T., Bohrmann, G., Plaza–Faverola, A., Bünz, S., et al. (2019). A 160,000-year-old history of tectonically controlled methane seepage in the Arctic. *Sci. Adv.* 5, eaaw1450. doi:10.1126/sciadv.aaw1450

Himmler, T., Smrzka, D., Zwicker, J., Kasten, S., Shapiro, R. S., Bohrmann, G., et al. (2018). Stromatolites below the photic zone in the northern Arabian Sea formed by calcifying chemotrophic microbial mats. *Geology* 46 (4), 339–342. doi:10.1130/G39890.1

Irwin, H., Curtis, C., and Coleman, M. (1977). Isotopic evidence for source of diagenetic carbonates formed during burial of organic-rich sediments. *Nature* 269, 209–213. doi:10.1038/269209a0

Jakobsson, M., Mayer, L., Coakley, B., Dowdeswell, J. A., Forbes, S., Fridman, B., et al. (2012). The international bathymetric chart of the arctic ocean (IBCAO) version 3.0. *Res. Lett.* 39, L12609. doi:10.1029/2012GL052219

Judd, A. G., Hovland, M., Dimitrov, L. I., Garcia, G. S., and Jukes, V. (2002). The geological methane budget at continental margins and its influence on climate change. *Geofluids* 2, 109–126. doi:10.1046/j.1468-8123.2002.00027.x

Kim, S.-T., O'Neil, J. R., Hillaire-Marcel, C., and Mucci, A. (2007). Oxygen isotope fractionation between synthetic aragonite and water: influence of temperature and Mg2+ concentration. *Geochem. Cosmochim. Acta* 71, 4704–4715. doi:10.1016/j.gca.2007.04.019

Leefmann, T., Bauermeister, J., Kronz, A., Liebetrau, V., Reitner, J., and Thiel, V. (2008). Miniaturized biosignature analysis reveals implications for the formation of cold seep carbonates at Hydrate Ridge (off Oregon, USA). *Biogeosciences* 5, 731–738. doi:10.5194/bg-5-731-2008

Lu, Y., Yang, X., Lin, Z., Sun, X., Yang, Y., and Peckmann, J. (2021). Reducing microenvironments promote incorporation of magnesium ions into authigenic carbonate forming at methane seeps: constraints for dolomite formation. *Sedimentology* 68, 2945–2964. doi:10.1111/sed.12919

Luff, R., Wallmann, K., and Aloisi, G. (2004). Numerical modeling of carbonate crust formation at cold vent sites: significance for fluid and methane budgets and chemosynthetic biological communities. *Earth Planet. Sci. Lett.* 221, 337–353. doi:10.1016/S0012-821X(04)00107-4

Lundschien, B. A., Mattingsdal, R., Johansen, S. K., and Knutsen, S.-M. (2023). "North Barents composite tectono-sedimentary element," in *Sedimentary successions of the arctic region and their hydrocarbon prospectivity*. Editors S. S. Drachev, H. Brekke, E. Henriksen, and T. Moore (London, Memoirs: Geological Society), 57. doi:10.1144/M57-2021-39

Naehr, T. H., Eichhubl, P., Orphan, V. J., Hovland, M., Paull, C. K., Ussler, W., III., et al. (2007). Authigenic carbonate formation at hydrocarbon seeps in continental margin sediments: a comparative study. *Deep-Sea Res. II Top. Stud. Oceanogr.* 54 (11–13), 1268–1291. doi:10.1016/j.dsr2.2007.04.010

Neuweiler, F., Rutsch, M., Geipel, G., Reimer, A., and Heise, K.-H. (2000). Soluble humic substances from *in situ* precipitated microcrystalline calcium carbonate, internal sediment, and spar cement in a Cretaceous carbonate mud-mound. *Geology* 28, 851–854. doi:10.1130/0091-7613(2000)28<851:shsfis>2.0.co;2

Peckmann, J., and Thiel, V. (2004). Carbon cycling at ancient methane–seeps. *Chem. Geol.* 205, 443–467. doi:10.1016/j.chemgeo.2003.12.025

Pohlman, J. W., Bauer, J. E., Canuel, E. A., Grabowski, K. S., Knies, D. L., Mitchell, C. S., et al. (2009). Methane sources in gas hydrate-bearing cold seeps: evidence from radiocarbon and stable isotopes. *Mar. Chem.* 115, 102–109. doi:10.1016/j.marchem.2009.07.001

Rasmussen, T. L., and Thomsen, E. (2021). Climate and ocean forcing of ice-sheet dynamics along the Svalbard-Barents Sea ice sheet during the deglaciation ~20,000–10,000 years BP. *Quat. Sci. Adv.* 3, 100019. doi:10.1016/j.qsa.2020.100019

Reeburgh, W. S. (2007). Oceanic methane biogeochemistry. *Chem. Rev.* 107 (2), 486–513. doi:10.1021/cr050362v

Riding, R. (2000). Microbial carbonates: the geological record of calcified bacterial–algal mats and biofilms. *Sedimentology* 47, 179–214. doi:10.1046/j.1365-3091.2000.00003.x

Ritger, S., Carson, B., and Suess, E. (1987). Methane-derived authigenic carbonates formed by subduction-induced pore-water expulsion along the Oregon/Washington margin. *Geol. Soc. Am. Bull.* 98, 147–156. doi:10.1130/0016-7606(1987)98<147:macfbs>2.0.co;2

Roberts, H. H., Feng, D., and Joye, S. B. (2010). Cold-seep carbonates of the middle and lower continental slope, northern Gulf of Mexico. *Deep-Sea Res. II* 57, 2040–2054. doi:10.1016/j.dsr2.2010.09.003

Sassen, R., Roberts, H. H., Carney, R., Milkov, A. V., DeFreitas, D. A., Lanoil, B., et al. (2004). Free hydrocarbon gas, gas hydrate, and authigenic minerals in chemosynthetic communities of the northern Gulf of Mexico continental slope: relation to microbial processes. *Chem. Geol.* 205, 195–217. doi:10.1016/j.chemgeo.2003.12.032

Sauer, S., Crémière, A., Knies, J., Lepland, A., Sahy, D., Martma, T., et al. (2017). U-Th chronology and formation controls of methane-derived authigenic carbonates from the Hola trough seep area, northern Norway. *Chem. Geol.* 470, 164–179. doi:10.1016/j.chemgeo.2017.09.004

Sejrup, H. P., Hjelstuen, B. O., Patton, H., Esteves, M., Winsborrow, M., Rasmussen, T. L., et al. (2022). The role of ocean and atmospheric dynamics in the marine-based collapse of the last Eurasian Ice Sheet. *Commun. Earth Environ.* 3, 119. doi:10.1038/s43247-022-00447-0

Sen, A., Åström, E. K. L., Hong, W.-L., Portnov, A., Waage, M., Serov, P., et al. (2018). Geophysical and geochemical controls on the megafaunal community of a high Arctic cold seep. *Biogeosciences* 15, 4533–4559. doi:10.5194/bg-15-4533-2018

Serov, P., Vadakkepuliyambatta, S., Mienert, J., Patton, H., Portnov, A., Silyakova, A., et al. (2017). Postglacial response of Arctic Ocean gas hydrates to climatic amelioration. *Proc. Natl. Acad. Sci. USA* 114 (24), 6215–6220. doi:10.1073/pnas.1619288114

Serov, P., Mattingsdal, R., Winsborrow, M., Patton, H., and Andreassen, K. (2023). Widespread natural methane and oil leakage from sub-marine Arctic reservoirs. *Nat. Commun.* 14, 1782. doi:10.1038/s41467-023-37514-9

Smrzka, D., Zwicker, J., Misch, D., Walkner, C., Gier, S., Monien, P., et al. (2019). Oil seepage and carbonate formation: a case study from the southern Gulf of Mexico. *Sedimentology* 66, 2318–2353. doi:10.1111/sed.12593

Suess, E. (2014). Marine cold seeps and their manifestations: geological control, biogeochemical criteria and environmental conditions. *Int. J. Earth Sci. Geol. Rundsch* 103, 1889–1916. doi:10.1007/s00531-014-1010-0

Teichert, B. M. A., Eisenhauer, A., Bohrmann, G., Haase-Schramm, A., Bock, B., and Linke, P. (2003). U/Th systematics and ages of authigenic carbonates from Hydrate Ridge, Cascadia Margin: recorders of fluid flow variations. *Geochim. Cosmochim. Acta* 67, 3845–3857. doi:10.1016/s0016-7037(03)00128-5

Thorsnes, T., Chand, S., Bellec, V., Nixon, F. C., Brunstad, H., Lepland, A., et al. (2023). Gas seeps in Norwegian waters – distribution and mechanisms. *Nor. J. Geol.* 103, 2. doi:10.17850/njg103-2-4

Waage, M., Portnov, A., Serov, P., Bünz, S., Waghorn, K. A., Vadakkepuliyambatta, S., et al. (2019). Geological controls on fluid flow and gas hydrate pingo development on the Barents Sea margin. *Geochem. Geophysics,Geosystems* 20, 630–650. doi:10.1029/2018GC007930

Waage, M., Serov, P., Andreassen, K., Waghorn, K. A., and Bünz, S. (2020). Geological controls of giant crater development on the Arctic seafloor. *Sci. Rep.* 10, 8450. doi:10.1038/s41598-020-65018-9

Weniger, P., Blumenberg, M., Berglar, K., Ehrhardt, A., Klitzke, P., Krüger, M., et al. (2019). Origin of near-surface hydrocarbon gases bound in northern Barents Sea sediments. *Mar. Petroleum Geology* 102, 455–476. doi:10.1016/j.marpetgeo.2018.12.036

Yao, H., Panieri, G., Lehmann, M. F., Himmler, T., and Niemann, H. (2021). Biomarker and isotopic composition of seep carbonates record environmental conditions in two arctic methane seeps. *Front. Earth Sci.* 8, 570742. doi:10.3389/feart.2020.570742

Zhang, F., Xu, H., Konishi, H., Kemp, J. M., Roden, E. E., and Shen, Z. (2012). Dissolved sulfide-catalyzed precipitation of disordered dolomite: implications for the formation mechanism of sedimentary dolomite. *Geochim. Cosmochim. Acta* 97, 148–165. doi:10.1016/j.gca.2012.09.008

Zwicker, J., Smrzka, D., Himmler, T., Monien, P., Gier, S., Goedert, J. L., et al. (2018). Rare earth elements as tracers for microbial activity and early diagenesis: a new perspective from carbonate cements of ancient methane-seep deposits. *Chem. Geol.* 501, 77–85. doi:10.1016/j.chemgeo.2018.10.010